Indian Journal of Pure & Applied Physics
Vol. 58, November 2020, pp. 825-831

Effect of CNT on the growth and agglomeration of TiO_2 nanoparticles

Hitesh Kumar Sharma[a#], Sanjeev K Sharma[*#a], Sanjeev Kumar[b] & Beer Pal Singh[**a]

[a]Nanomaterials Laboratory, Department of Physics, Ch. Charan Singh University, Meerut, UP-250 004, India

[b]Department of Physics, Rajiv Gandhi University, Doimukh, Itanagar, Arunachal Pradesh 791112, India

#Equal Contributor and First Author

Received 26 July 2020; accepted 30 September 2020

Titanium dioxide nanoparticles (TiO_2-NPs) are agglomerated by inclusion of CNTs during the nucleation and growth process using the hydrothermal method at 160 ºC. The content of C-atoms was determined from EDAX-spectra and line scan. The XRD peak of TiO_2 indicated the rutile phase R(210), while CNT- TiO_2 showed the anatase phase A(004). Williamson-Hall (W-H) models showed the linear fitted negative slope, indicated the presence of compressive strain in TiO_2 and CNT- TiO_2 crystal lattice. Agglomeration of TiO_2 nanoparticles was confirmed from the surface morphology and elemental analysis. The FTIR spectra showed the interfacial interaction between CNTs and TiO_2 with vibrational frequency of Ti-O-C bonds at 1065 cm^{-1}.

Keywords: Agglomeration of TiO_2 nanoparticles; Williamson- Hall analysis and Size-strain Plot method; Elemental composition and functional sites.

1 Introduction

Titanium dioxide (TiO_2) has shown the great importance in the production of various modern products like UV protected layers either sunglass or sun-cream, self-cleaning and antiglare screens, photo catalytic extraordinary performance, drug delivery and so on[1-4]. TiO_2 has the semiconducting properties and used in many electronic devices like solar-cells, photo catalytic activity due to a wide band gap (E_g = 3.2 eV), low cost, non-toxic, chemical and thermal stability[5-7]. Photo catalytic properties and other applications of nanostructured TiO_2 depend on the crystallinity, morphology and the dopant concentration[8]. Defects created in TiO_2 lattice by making the composite or the dopant concentration leads to broadening and shifting of diffraction peaks, which can give the information for particular applications[9, 10]. There are many nucleation and growth methods of TiO_2 have been reported in the literature[11-13]. All of them, the hydrothermal method for the synthesis of nanostructured TiO_2 can be preferred due to ease of the alteration of the microstructure and dopant concentration[14-16]. There are two major geometrical parameters like lattice strains or defects by vacancies or interstitial can be estimated from XRD peak profile analysis[17,18]. A roadmap for the determination of strains of nanostructured TiO_2 has been reported with the explanation of intrinsic defects (oxygen/titanium vacancies and interstitials), metallic dopants or non-metallic dopants (carbon)[19]. The crystallite size and lattice strain induced the broadening of diffraction peak intensity or shifting the peak position. Williamson-Hall models and size-strain plot method are simplified the structural parameters, where the crystallite size, residual stress and energy density can be determined by considering the peak width as a function of diffraction angle[20, 21]. Rajender *et al*. have reported the strain induced phase formation and microstructural analysis of TiO_2 determined by the uniform deformation model[22]. Chenari *et al*. evaluated physical parameters of TiO_2 such as strain, stress and energy density using Williamson-Hall (W-H) plot assuming a uniform deformation model (UDM), and uniform deformation energy density model (UDEDM)[23]. Islam *et al*. estimated the crystalline structure of ZnO-doped TiO_2 nanoparticles from Williamson-Hall (W-H) model and size-strain plot (SSP) method[24]. Despite the comprehensive structural parameters of TiO_2 estimated from W-H models and SSP method, the strain, stress and energy density of CNTs based agglomerated TiO_2 nanoparticles are fewer studied.

The objective of this research work is to synthesize agglomerated TiO_2 nanoparticles by the hydrothermal method at 160 °C and estimated the structural

Corresponding Author: *sksharma18@ccsuniversity.ac.in, **drbeerpal@gmail.com

parameters from Williamson-Hall analysis as uniform deformation model (UDM), uniform stress deformation model (USDM), uniform deformation energy density model (UDEDM) and size strain plot (SSP) method. The effect of CNTs for the agglomeration of TiO_2 nanoparticles is analyzed from the field emission-scanning electron microscopy (FE-SEM), energy dispersive X-ray analysis (EDAX) spectra and line scan. While the functional cites of nanostructured TiO_2 and CNT-TiO_2 were determined from FTIR spectroscopy.

2. Experimental

2.1 Synthesis of agglomerated TiO_2 nanoparticles

TiO_2 nanoparticles and agglomerated CNT-TiO_2 nanocomposite were synthesized by the hydrothermal method. Firstly 0.1M solution was prepared from the precursor of titanium tetra isopropoxide (TTIP) solution and the glacial acetic acid (GAA). The prepared solution was stirred at room temperature for 5 min. The dilute solution of sodium dodecyl sulphate (SDS) was mixed with TTIP-GAA solution at room temperature. The diluted HCl solution was added drop by drop into TTIP-GAA-SDS solution and stirred with magnetic stirrer at room temperature for 15 min. To check the effect of CNTs, 0.5 mg was added in the growth process. The hydrothermal reactions take place at 160 ℃ for 4 h. The synthesized precipitates were filtered, washed with deionized (DI) water several times and dried in an electric oven at 60 ℃.

2.2 Characterization of agglomerated CNT-TiO_2 nanocomposite

The structural analysis of TiO_2 nanoparticles and CNT-TiO_2 nanocomposite were determined from X-ray diffractometer (XRD: Rigaku) with Cu-Kα_1 radiation of wavelength 0.15406 nm at the scanning rate 0.1 deg/sec. The microstructures of TiO_2 and CNT-TiO_2 powders were determined from field emission-scanning electron microscopy (FE-SEM: Zeiss), at an accelerating voltage of 15 kV. The elemental composition of TiO_2 nanoparticles and CNT-TiO_2 nanocomposite was determined from energy dispersive X-ray analysis (EDAX) spectra and line scanning. The chemical bonding and functional cites were determind from FTIR spectroscopy (Agilent 630, ATR Module).

3. Results and Discussion

3.1 X-ray diffraction of TiO_2 nanoparticles and CNT-TiO_2 nanocomposite

Figure 1 shows the XRD pattern of CNT, TiO_2 nanoparticles and CNT-TiO_2 nanocomposite. All diffraction peaks indicated the mixture of anatase and rutile phases of TiO_2, indexed with the reference data of JCPDS file (rutile: 00-002-0494 and anatase: 00-002-0387), which confirmed the tetragonal structure of TiO_2. Lattice parameters were estimated from XRD peak profile analysis and summarized in Table 1.

XRD pattern of TiO_2 and CNT-TiO_2 clearly showed the difference in diffraction peak intensities. The diffraction peaks intensity of CNT-TiO_2 nanocomposite was deteriorated by adding a small amount of CNTs during the growth of nanostructured TiO_2. The dominant peak of TiO_2 indicated the rutile phase R (210). While the addition of CNTs in TiO_2 nanoparticles, the dominant peak was observed the anatase phase A(004). The transformation of crystallographic structure induced the rearrangement of atoms in lattices. The arrangement of atoms was reversed due to the creation of defects or oxygen vacancies in the lattices by addition of CNTs during the growth process. Defects and oxygen vacancies are responsible factors for the trapping of electrons and holes[25, 26]. The crystallite size, residual stress and uniform energy density, were estimated from the following analysis models and methods.

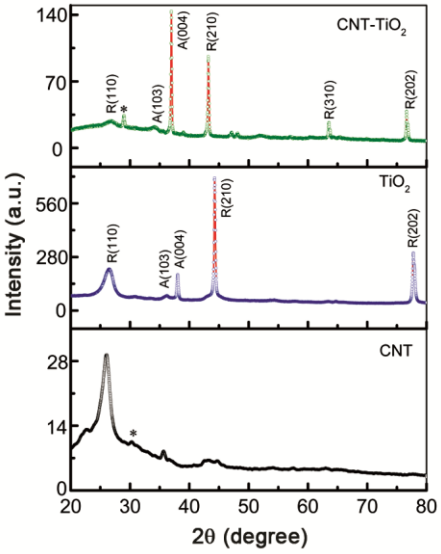

Fig. 1 — XRD pattern of CNT, TiO_2 nanoparticles and CNT-TiO_2 nanocomposite.

Table 1 — Lattice parameters of TiO_2nanoparticles and CNT-TiO_2 nanocomposite.

S. No.	Lattice parameters	TiO_2	CNT-TiO_2
1	a = b (Å)	4.5728	4.6838
2	c(Å)	2.9087	9.7033
3	c/a ratio	0.6361	2.0717
4	d (Å)	2.0432	2.4289

3.1.1 X-ray peak broadening analysis: crystallite size by Scherrer's formula

The peak broadening is related to the crystallite size and lattice strain presented in the material as well as instrumental measurement errors. The broadening, β_{hkl} corresponding to the diffraction peak of TiO_2 is given by the following relation:

$$\beta_{hkl} = \left(\beta^2_{measured} - \beta^2_{instrumental}\right)^{1/2} \quad \ldots (1)$$

The crystallite size D, of TiO_2 nanoparticles and CNT-TiO_2 nanocomposite was calculated by the Scherrer's formula:

$$D = \frac{k\lambda}{\beta_D cos\theta} \quad \ldots (2)$$

where, k is constant (for spherical shape k = 0.9), λ is wavelength of X-rays (0.15406 nm), β_D is full width at half maximum and θ is the diffraction angle.

3.1.2 Williamson-Hall analysis

3.1.2.1 Uniform deformation model (UDM)

The crystallite size, D, lattice strain ε, induced broadening, β_s, of nanostructured TiO_2 were determined from the following relation[27]:

$$\beta_s = 4\varepsilon \tan\theta \quad \ldots (3)$$

The crystallite size-induced Bragg's broadening (β_D) is described by rearranging Eq^n. (2),

$$\beta_D = \frac{k\lambda}{Dcos\theta} \quad \ldots (4)$$

The combined effect of broadening (β_{hkl}) is govern by :

$$\beta_{hkl} = \beta_s + \beta_D \quad \ldots (5)$$

Using Eq. 3 and 4 in Eq. 5, we get

$$\beta_{hkl} = 4\varepsilon \tan\theta + \frac{k\lambda}{Dcos\theta} \quad \ldots (6)$$

By rearranging Eq. 6,

$$\beta_{hkl} cos\theta = \frac{k\lambda}{D} + 4\varepsilon \sin\theta \quad \ldots (7)$$

The UDM plots are obtained by plotting $4sin\theta$ on x-axis and $\beta_{hkl}cos\theta$ on y- axis for TiO_2 nanoparticles and CNT-TiO_2 nanocomposite as shown in Figs. 2(a & b). The slope of linear fitted data gives the information of the lattice strain and crystallite size, which can be extracted from the y-intercept. The negative slope of linear fitted data shows the presence of compressive strain in the material[28].

3.1.2.2 Uniform stress deformation model (USDM)

The USDM model was considered for the evaluation of the stress raised in the material due to the lattice deformation in all crystallographic directions. According to Hook's law (within the elastic limits), the stress is linearly proportional to the strain.

$$\sigma = E\varepsilon \quad \ldots (8)$$

where, σ is the stress of the crystal lattice and E is the modulus of elasticity called as Young's modulus. The above relation (Eq. 8) is valid for small strains presented in nanostructured TiO_2[20]. Using Hook's low, in Eq. 7 the stress is described as following:

$$\beta_{hkl} cos\theta = \frac{k\lambda}{D} + \frac{4\sigma \sin\theta}{E_{hkl}} \quad \ldots (9)$$

The Young's modulus, E_{hkl} in the direction normal to the set of (hkl) of tetragonal crystal system (TiO_2) is given by the following relation[29]:

$$E^{-1}_{hkl} = \frac{1}{(h^2+k^2+L^2)^2}\left[\begin{array}{l} S_{11}(h^4+k^4)+(2S_{12}+S_{66})h^2k^2 + \\ (2S_{13}+S_{44})(h^2+k^2)L^2 + S_{33}L^4 \end{array}\right] \quad \ldots (10)$$

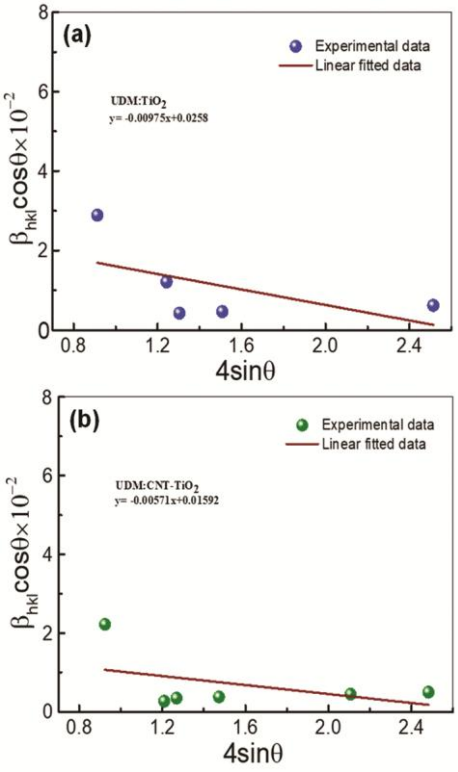

Fig. 2 — The W-H analysis (UDM) of (a) TiO_2 nanoparticles and (b) CNT-TiO_2 nanocomposite.

where $L=\left(\frac{a}{c}l\right)$, and S_{11}, S_{12},S_{13}, S_{33}, S_{44}, andS_{66} are elastic compliances with their standard values of 5.1 $(TPa)^{-1}$, -0.8 $(TPa)^{-1}$, -3.3$(TPa)^{-1}$, 10.7$(TPa)^{-1}$, 18.5 $(TPa)^{-1}$ and 16.7 $(TPa)^{-1}$ for anatase TiO_2 and 6.8 $(TPa)^{-1}$, -4 $(TPa)^{-1}$, -0.85 $(TPa)^{-1}$, 2.60 $(TPa)^{-1}$, 8.06 $(TPa)^{-1}$, and 5.21 $(TPa)^{-1}$ for rutile TiO_2 nanoparticles respectively[21, 22]. The average calculated young's modulus are 223 GPa and 199 GPa for TiO_2 nanoparticles and CNT-TiO_2 nanocomposite, respectively. The effect of decreasing of Young's modulus for CNT-TiO_2 nanocomposite was observed due to increasing the crystallite size or the agglomeration of NPs[30]. Figs. 3(a & b) show the USDM plot ($4sin\theta/E_{hkl}$ versus $\beta_{hkl}cos\theta$) for TiO_2 nanoparticles and CNT-TiO_2 nanocomposite, respectively. The stress is calculated from the slope and crystallite size from y-intercept of linearly fitted data.

3.1.2.3 Uniform deformation energy density model (UDEDM)

The UDEDM is used to determine the energy density (energy/unit volume) of the crystal lattice. The uniform stress deformation model is considered for homogeneous and isotropic crystals. The assumption of homogeneity and isotropy is no longer exists throughout the crystal lattice. In this model, the crystal lattice is assumed to have anisotropic nature. The constants of proportionality associated with the stress-strain relation are no longer independent, when the strain energy density 'u' is considered. By Hooke's law, the anisotropic energy density is related as $u=\varepsilon^2 E_{hkl}/2$. Therefore, the Eq. 7 can be modified as following[20]:

$$\beta_{hkl}cos\theta=\frac{k\lambda}{D}+4sin\theta\left(\frac{2u}{E_{hkl}}\right)^{1/2} \quad \ldots (11)$$

Figure 4(a & b) show the UDEDM plots ($4sin\theta(2/E_{hkl})^{1/2}$ versus $\beta_{hkl}cos\theta$) of TiO_2 nanoparticles and CNT-TiO_2 nanocomposite, respectively. The anisotropic energy density is determined from the slope and the crystallite size from y-intercept of linear fitted data. Further, the lattice strain can be calculated from σ/E_{hkl} and stress from the relation $u=\sigma^2/E_{hkl}$.

3.1.3 Size-strain plot (SSP) method

For isotropic line broadening, the size-strain plot (SSP) method was also considered for the better evaluation of crystallite size and micro-strains. It was expected that the crystallite size and the strain profile is defined by Lorentzian function and Gaussian function respectively[31].

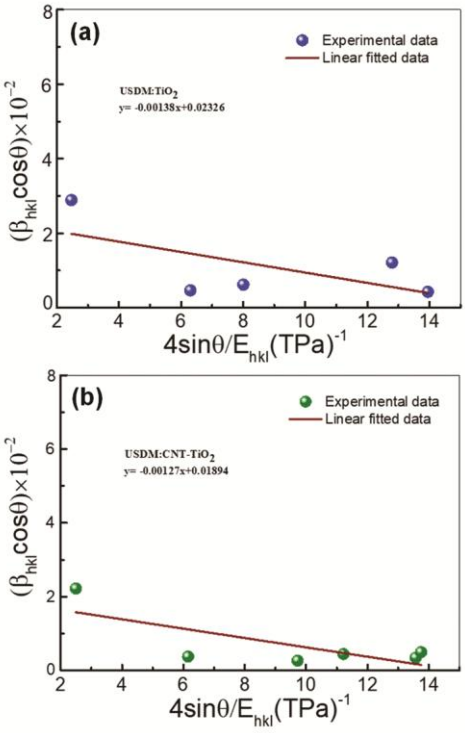

Fig. 3 — The modified W-H analysis (USDM) of (a) TiO_2 nanoparticles and (b) CNT-TiO_2 nanocomposite.

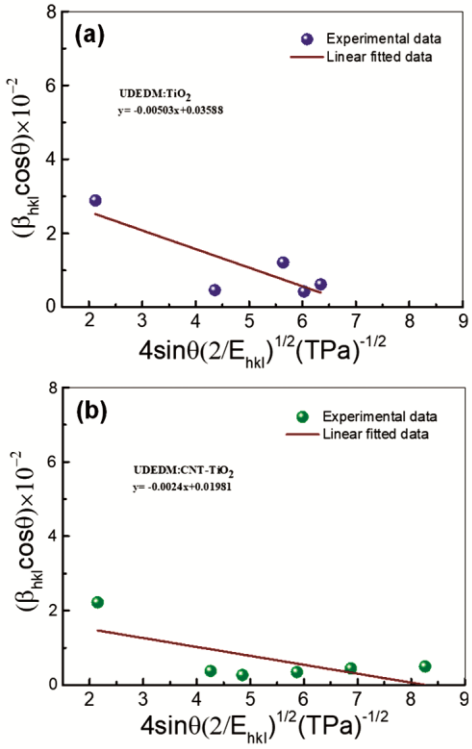

Fig. 4 — The modified W-H analysis (UDEDM) of (a) TiO_2nanoparticles and (b) CNT-TiO_2 nanocomposite.

$$\left(d_{hkl}\beta_{hkl}cos\theta/\lambda\right)^2 = \frac{k}{D}\left(d_{hkl}^2\beta_{hkl}cos\theta/\lambda\right)+\left(\frac{\varepsilon}{2}\right)^2 \quad \ldots (12)$$

where k is constant; for sphere like shape it has the value of ¾. Figs. 5(a & b) show the strain-size plots ($\left(d_{hkl}^2\beta_{hkl}cos\theta/\lambda\right)$ versus $\left(d_{hkl}\beta_{hkl}cos\theta/\lambda\right)^2$) of TiO_2 nanoparticles and CNT-TiO_2 nanocomposite, respectively. The crystallite size was estimated from the slope of the linearly fitted data and the square root of the y-intercept gives the strain.

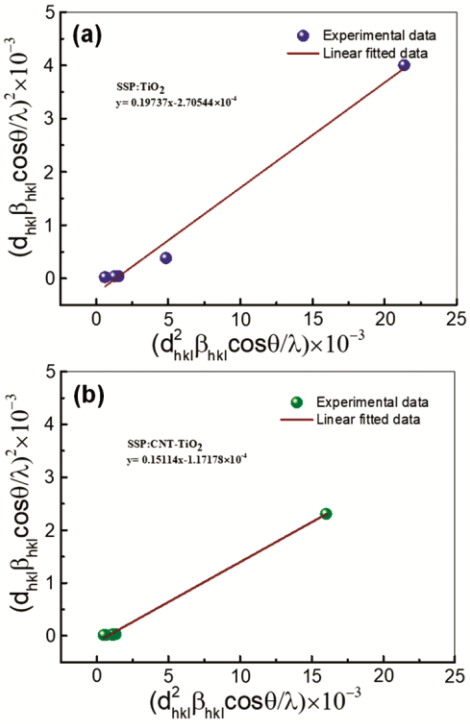

Fig. 5 — The size- strain plot (SSP) analysis of (a) TiO_2 nanoparticles and (b) CNT-TiO_2 nanocomposite.

All results estimated from the various methods and models (Scherrer's method, UDM, USDM, UDEDM models and SSP) are summarized in Table 2.

For all W-H models, the slope of linear fitted data was observed the negative slop, which indicated the presence of compressive strain in TiO_2 and CNT-TiO_2 crystal lattice. Even though, the crystallite size was observed in good agreement evaluated from all models and methods.

3.2 Microstructure and elemental analysis of CNT-TiO_2 nanocomposite

Figures 6(a - c) shows the microstructure (FE-SEM images) of CNT, TiO_2 nanoparticles, and agglomerated CNT-TiO_2 nanocomposite, respectively. The diameter of CNT was observed to be ~35 nm. The magnified images of CNTs, TiO_2 and CNT-TiO_2 are inset of each microstructure. The microstructure of TiO_2 is clearly showed the inaccessible nano-grains. While the addition of CNTs in the nucleation and growth of nano structured TiO_2, the agglomeration of nanoparticles were observed, which is clearly reflected from the images. The average crystallite size increased from 29 nm to 40 nm as the microstructure transformed from TiO_2 to CNT-TiO_2, which was estimated from the Scherrer's formula. The elemental analysis of CNTs, TiO_2 and CNT-TiO_2 was determined using an energy dispersive X-ray analysis (EDAX) spectra and line scanning (Fig. S1(a-c)). When CNTs was introduced in the growth of TiO_2, the elemental distribution of Ti and O atoms was observed the least homogeneous (Fig. S2(b)). The inhomogeneous pattern revealed the interaction of C atom with Ti and O atoms generating new carbonaceous chemical bonds as Ti-C or Ti-O-C[32, 33]. The EDAX line scanning pattern are also justified with EDAX spectra (Fig. S1).

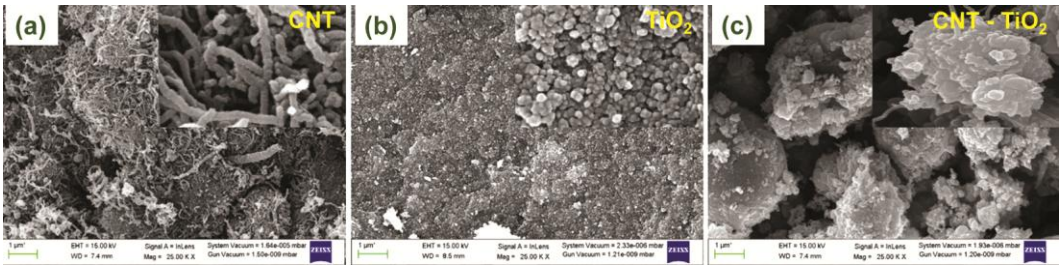

Fig. 6 — FE-SEM images of (a) CNT, (b) TiO_2 nanoparticles and (c) CNT-TiO_2 naocomposite.

Table 2 — Geometric parameters of TiO_2nanoparticles and CNT-TiO_2 nanocomposite.

S. No	Sample Name	Scherrer's Method	Williamson-Hall Method									SSP			
			UDM		USDM			UDEDM							
		D (nm)	D (nm)	ε x10^{-2}	D (nm)	ε x10^{-2}	σ (MPa)	D (nm)	ε x10^{-2}	σ (MPa)	U (MPa)	D (nm)	ε x10^{-2}	σ (MPa)	U (MPa)
1	TiO_2	29.88	5.37	0.975	5.96	0.619	1380	3.86	1.065	2374	25.301	3.80	3.290	7328	241.000
2	CNT-TiO_2	40.14	8.71	0.571	7.32	0.637	1270	6.99	0.538	1071	5.76	4.96	2.165	4315	93.414

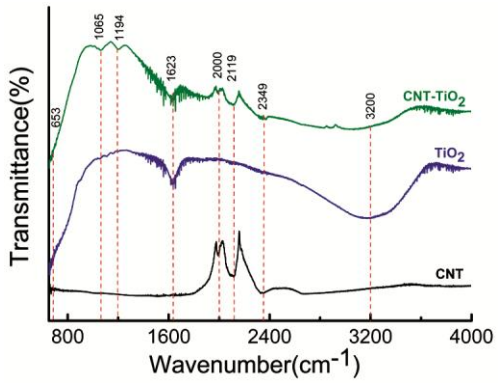

Fig. 7 — FTIR spectra of CNT, TiO_2 nanoparticles, and CNT-TiO_2 nanocomposite.

3.3 FTIR of TiO_2 nanoparticles and CNT-TiO_2 nanocomposite

Figure 7 shows the FTIR spectra of CNTs, TiO_2 nanoparticles and CNT-TiO_2 nanocomposite for the analysis of chemical bondings.The fundamental vibrations of TiO_2 nanoparticles was appeared near 653 cm^{-1}, which is attributed to the stretching vibration of Ti-O bonds[34]. Another vibration was detected at 1065 cm^{-1} assigned to Ti-O-C bonds for the interaction between TiO_2 and CNT[32]. The stretching vibration for C-O was observed at 1194 cm^{-1} [35]. Another peak was observed at 1623 cm^{-1}, that is ascribed to C=C bond for the stretching of CNT. The C-H bending was found at ~2000 cm^{-1}. The peak was observed at 2119 cm^{-1} stem from CNT[36, 37]. The additional band edge was observed at 2349 cm^{-1} ascribed to physically adsorbed CO_2 from the atmosphere. The vibrations near frequency 3200 cm^{-1} assigned to the -OH stretching group[38].

The agglomeration of TiO_2 nanoparticles depends on the growth parameters like growth temperature, pressure, volume in autoclave, molarity as well as the dopant material. The dopant material plays a very significant role in the growth of nanoparticles by creating new bonds and defects[39]. The particles with lower energy density get to achieve the more stable geometrical shape or agglomeration on any particular surface. When CNTs were used as the dopant material in the solution, it reduced the energy density. The energy density or energy/unit volume for CNT-TiO_2 nanocomposite is less than that of TiO_2 nanoparticles estimated from uniform deformation energy density model (UDEDM) and size-strain plot (SSP) method and particles get agglomerated on CNT surface.

4. Conclusion

Nanostructured TiO_2 and CNT-TiO_2 were synthesized successfully using the hydrothermal method at the nucleation and growth temperature of 160 °C. XRD-pattern confirmed the mixed phase of anatase and rutile of TiO_2. Agglomeration of TiO_2 nanoparticles by inclusion of CNT was confirmed from XRD pattern and FE-SEM images. The presence of C-content in agglomerated nanostructured TiO_2 was confirmed from EDAX-spectra and line scanning. The crystallite size, D, and lattice stains, ε, estimated from the Scherrer's formula, and W-H models. The UDEDM model clarified the decrease in energy density of CNT-TiO_2 nanocomposite, specified the agglomeration of TiO_2 nanoparticles. FTIR spectra confirmed the different functional stretching and bending with particular vibrational frequencies.

Acknowledgment

The authors are thankful to Department of Science and Technology, Govt. of India for instrumentation facilities under DST-FIST project (SR/FST/PSI-177/2012) at Department of Physics, Ch. Charan Singh University, Meerut, UP, India.

References

1 Rahimi N, Pax R A & Gray E M, *Progress Solid State Chem*, 44 (2016) 86.
2 Ali I, Suhail M, Alothman Z A & Alwarthan A, *RSC Advances*, 8 (2018) 30125.
3 Song Y Y, Schmidt-Stein F, Bauer S & Schmuki P, *J Am Chem Soc*, 131 (2009) 4230.
4 Wang T, Jiang H, Wan L, Zhao Q, Jiang T, Wang B & Wang S, *Acta Biomaterialia*, 13 (2015) 354.s
5 Kusior A, Banas J, Trenczek-Zajac A, Zubrzycka P, Micek-Ilnicka A & Radecka M, *J Mol Struct*, 1157 (2018) 327.
6 He Z, Que W W X & Xie H, Titanium dioxide: Structure, properties and applications, (2013) 1.
7 Barringer E A & Bowen H K, *Langmuir*, 1 (1985) 414.
8 Bahmanrokh G, Cazorla C, Mofarah S S, Shahmiri R, Yao Y, Ismail I, Chen W F, Koshy P & Sorrell C C, *Nanoscale*, 12 (2020) 4916.
9 Murashkina A A, Murzin P D, Rudakova A V, Ryabchuk V K, Emeline A V & Bahnemann D W, *The J Phys Chem C*, 119 (2015) 24695.
10 Zahid R, Manzoor M, Rafiq A, Ikram M, Nafees M, Butt A R, Hussain S G & Ali S, *Electron Mater Lett*, 14 (2018) 587.
11 Mehranpour H, Askari M & Ghamsari M S, Nucleation and Growth of TiO2 Nanoparticles, 2011.
12 Verma R, Gangwar J & Srivastava A K, *RSC Advances*, 7 (2017) 44199.
13 Zhang B, Cao S, Du M, Ye X, Wang Y & Ye J, *Catalysts*, 9 (2019) 91.
14 Mehnane H F, Wang C, Kondamareddy K K, Yu W, Sun W, Liu H, Bai S, Liu W, Guo S & Zhao X Z, *RSC Advances*, 7 (2017) 2358.
15 Xuelian X & Junjiang Z, *Recent Patents Chem Eng*, 5 (2012) 134.

16 Cano-Casanova L, Amorós-Pérez A, Lillo-Ródenas M Á & Román-Martínez M C, *Materials*, 11 (2018) 2227.
17 Riazian M, Rad S & Azinabadi R, *J Kor Phys Soc*, 62 (2013).
18 Ali T, Ahmed A, Alam U, Uddin I, Tripathi P & Muneer M, *Mater Chem Phys*, 212 (2018).
19 Kelaidis N, Kordatos A, Christopoulos S R G & Chroneos A, *Sci Rep*, 8 (2018) 12790.
20 Zak A K, Majid W H A, Abrishami M E & Yousefi R, *Solid State Sci*, 13 (2011) 251.
21 Seetharaman A & Dhanuskodi S, *Spectrochimica Acta Part A: Mol Biomol Spectrosc*, 127 (2014) 543.
22 Rajender G & Giri P K, *J Alloys Compd*, 676 (2016) 591.
23 Chenari H M, Seibel C, Hauschild D, Reinert F & Abdollahian H, *Mater Res*, 19 (2016).
24 Islam M M, Alam M S, Choudhury M S H, Soga T, Yousuf A & Abuelwafa A A, Crystallite structure estimation of TiO2 doped ZnO nanoparticles from X-ray diffraction data, 5th International Conference on Advances in Electrical Engineering (ICAEE), (2019) 838.
25 Uratani H & Yamashita K, *The J Phys Chem Lett*, 8 (2017) 742.
26 Zhou Z, Liu J, Long R, Li L, Guo L & Prezhdo O V, *J Am Chem Soc*, 139 (2017) 6707.
27 Kaur N, Sharma S K & Kim D Y, *Curr Appl Phys*, 16 (2016) 231.
28 Yogamalar R, Srinivasan R, Vinu A, Ariga K & Bose A C, *Solid State Commun*, 149 (2009) 1919.
29 Jian-Min Z, Yan Z, Ke-Wei X & Vincent J, *Chin Phys B*, 17 (2008) 1565.
30 Patel G R & Pandya T C, *AIP Conf Proc*, 1837 (2017) 040024.
31 Tagliente M A, Massaro M, *Nucl Instrum Meth Phys Res B*, 266 (2008) 1055.
32 Huo K, Hu Y, Ma Y, Lü Y, Hu Z & Chen Y, *Nanotechnology*, 18 (2007) 145615.
33 Liu B, Huang Y, Wen Y, Du L, Zeng W, Shi Y, Zhang F, Zhu G, Xu X & Wang Y, *J Mater Chem*, 22 (2012) 7484.
34 Bezrodna T, Puchkovska G, Shymanovska V, Baran J & Ratajczak H, *J Mol Struct*, 700 (2004) 175.
35 Moya A, Cherevan A, Marchesan S, Gebhardt P, Prato M, Eder D & Vilatela J J, *Appl Catal B: Environ*, 179 (2015) 574.
36 Marković Z, Jovanović S, Kleut D, Romčević N, Jokanović V, Trajković V & Todorović-Marković B, *Appl Surf Sci*, 255 (2009) 6359.
37 Arora N, Banat F, Bharath G & Alhseinat E, *J Phys D: Appl Phys*, 52 (2019) 455304.
38 Estahbanati M R K, Feilizadeh M, Yancheshmeh M S & Iliuta M C, *Indus Eng Chem Res*, 58 (2019) 2770.
39 Khan M A M, Siwach R, Kumar S & Alhazaa A N, *Opt Laser Technol*, 118 (2019) 170.